Available online at www.sciencedirect.com
SCIENCE DIRECT®
Journal of Solid State Chemistry 177 (2004) 3700–3708
JOURNAL OF SOLID STATE CHEMISTRY
www.elsevier.com/locate/jssc

Multianvil high-pressure/high-temperature preparation, crystal structure, and properties of the new oxoborates $Dy_4B_6O_{14}(OH)_2$ and $Ho_4B_6O_{14}(OH)_2$

Hubert Huppertz*

Department Chemie und Biochemie, Ludwig-Maximilians-Universität München, Butenandtstraße 5-13 (Haus D), 81377 München, Germany

Received 11 May 2004; received in revised form 14 June 2004; accepted 17 June 2004
Available online 25 August 2004

Abstract

This paper reports about two new hydrogen-containing rare-earth oxoborates $RE_4B_6O_{14}(OH)_2$ (RE = Dy, Ho) synthesized under high-pressure/high-temperature conditions from the corresponding rare-earth oxides, boron oxide, and water using a Walker-type multianvil equipment at 8 GPa and 880 °C. The single crystal structure determination of $Dy_4B_6O_{14}(OH)_2$ showed: *Pbcn*, $a = 1292.7(2)$, $b = 437.1(2)$, $c = 887.3(2)$ pm, $Z = 2$, $R1 = 0.0190$, and w$R2 = 0.0349$ (all data). The isotypic holmium species revealed: *Pbcn*, $a = 1292.8(2)$, $b = 436.2(2)$, $c = 887.1(2)$ pm, $Z = 2$, $R1 = 0.0206$, and w$R2 = 0.0406$ (all data). The compounds exhibit a new type of structure, which is built up from layers of condensed BO_4-tetrahedra. Between the layers, the rare-earth cations are coordinated by 7 + 2 oxygen atoms. Furthermore, we report about temperature-resolved in situ powder diffraction measurements, DTA/TG, and IR-spectroscopic investigations into $RE_4B_6O_{14}(OH)_2$ (RE = Dy, Ho).

Keywords: High-pressure; Multianvil; $Dy_4B_6O_{14}(OH)_2$; $Ho_4B_6O_{14}(OH)_2$; Borates; Crystal structure

1. Introduction

In the last years, the focus of our interest was pointed towards the discovery of new metastable high-pressure phases in the area of anhydrous rare-earth oxoborates. The installation of a multianvil equipment at the Department Chemie of the Ludwig-Maximilians-University Munich (Germany) enabled us to perform systematic investigations in this field, taking advantage of increased pressure- and temperature-ranges [1,2]. Next to the synthesis of new polymorphs like χ-$RE$$BO_3$ (RE = Dy, Ho, Er), which contain layers built up from non-cyclic $[B_3O_9]^{9-}$-anions [3] or new *meta*-oxoborates like $RE(BO_2)_3$ (RE = Dy–Lu) [4], we were able to synthesize new compositions like $RE_4B_6O_{15}$ (RE = Dy, Ho) [5–7], α-$RE_2B_4O_9$ (RE = Eu, Gd, Tb, Dy) [8,9], and β-$RE_2B_4O_9$ [10] under extreme high-pressure/high-temperature conditions. In the cases of $RE_4B_6O_{15}$ (RE = Dy, Ho) and α-$RE_2B_4O_9$ (RE = Eu, Gd, Tb, Dy) the new structural motif of edge-sharing BO_4-tetrahedra was observed for the first time.

Research on the formation-range of the rare-earth oxoborates $RE_4B_6O_{15}$ (RE = Dy, Ho) led to the understanding that for the synthesis of $Dy_4B_6O_{15}$ a minimum pressure of 7 GPa and a temperature larger than 1000 °C were necessary. In the range 5–7 GPa, the system favored the formation of α-$Dy_2B_4O_9$ [9]. Additionally, we observed different reaction products, when temperature was lowered beneath 1000 °C (at 8 GPa). By a skilful adjustment of the synthetic parameters, it was possible to synthesize new hydrogen-containing products with the composition $RE_4B_6O_{14}(OH)_2$ (RE = Dy, Ho).

The search for hydrogen containing rare-earth oxoborates succeeded only in a few cases, e.g., hydrated

*Fax: +49-89-2180-77440.
E-mail address: huh@cup.uni-muenchen.de (H. Huppertz).

0022-4596/$ - see front matter © 2004 Elsevier Inc. All rights reserved.
doi:10.1016/j.jssc.2004.06.026

meta-oxoborates with the composition $RE(BO_2)_3 \cdot 6H_2O$ were precipitated by mixing 0.1 N solutions of rare-earth chlorides $RECl_3$ (RE = Y to Yb, except Pm, Eu, Tb, and Tm) and $Na_2B_4O_7$ at pH 6.6–6.8 and dried at 60 °C [11]. Further heating (80 °C) of the hexahydrates resulted in the formation of tetrahydrates $RE(BO_2)_3 \cdot 4H_2O$ [12]. No structural information is available about these phases. Recently, Lin et al. [13] reported the synthesis of hydrated rare-earth oxoborates with the composition $REB_6O_9(OH)_3$ (RE = Sm–Lu), using molten boric acid as reaction medium. The crystal structures contain a six-membered ring B_6O_{15} as a fundamental fragment. In a following publication, Lin et al. reported about two additional hydrated phases with the compositions $REB_8O_{11}(OH)_5$ (RE = La–Nd) and $REB_9O_{13}(OH)_4$ (RE = La–Nd) $\cdot 2H_2O$ [14]. They annealed these hydrated polyborates at moderate temperature to anhydrous pentaborates with the composition α-REB_5O_9 for RE = Pr–Eu and β-REB_5O_9 for RE = La, Ce. In all mentioned hydrated phases it was not possible to locate the hydrogen atoms from the structure refinements.

In this paper, we report about the syntheses, structures, and properties of the new rare-earth oxoborates $RE_4B_6O_{14}(OH)_2$ (RE = Dy, Ho). These phases represent hydrogen-containing intermediate phases on the way to the formation of the hydrogen-free high-pressure oxoborates $RE_4B_6O_{15}$ (RE = Dy, Ho).

2. Experimental part

According to Eq. (1), the new compounds $RE_4B_6O_{14}(OH)_2$ (RE = Dy, Ho) were synthesized from Dy_2O_3 (99.9%, Sigma-Aldrich, Taufkirchen), B_2O_3 (from H_3BO_3 (99.8%, Merck, Darmstadt) fired at 600 °C), and water:

$$2RE_2O_3 + 3B_2O_3 + H_2O \xrightarrow[880\,^\circ C,\ 10\ min]{8.0\ GPa} RE_4B_6O_{14}(OH)_2 \quad (RE = Dy,\ Ho). \tag{1}$$

As dysprosium oxide and boron oxide were mixed thoroughly under air, the water added itself by partial hydrolysis of the boron oxide. Alternatively, water was added using a micropipette. Each mixture was loaded into a 3.66 mm outside diameter, 0.33 mm wall thickness, and 6.0 mm length hexagonal boron nitride cylinder, that was sealed by a BN plate. The sample cylinder was placed into the center of a cylindrical resistance heater (graphite), that had a variable (stepped) wall thickness in order to minimize the thermal gradient along the sample [15–17]. MgO rods filled the space at the top and the bottom of the sample. A cylindrical zirconia sleeve surrounding the furnace provided thermal insulation. As pressure medium, Cr_2O_3-doped MgO octahedra (Ceramic Substrates & Components LTD., Isle of Wight) with an edge length of 18 mm were used. A hole was drilled in the octahedron, the cylindrical assembly positioned inside and contacted with a molybdenum ring at the top and a molybdenum plate at the bottom. The experimental temperature was monitored using a $Pt/Pt_{87}Rh_{13}$ thermocouple, that was inserted axially into the octahedral assembly, the hot junction in contact with the boron nitride cylinder. Eight tungsten carbide cubes, separated by pyrophyllite gaskets (Plansee, Reutte, TSM10, edge length: 32 mm), with a truncation of 11 mm were used to compress the octahedron (“18/11 assembly” in conventional terminology) via a modified Walker-style split-cylinder multianvil apparatus [1,2]. For further details of the Walker-type module and multianvil experiments see [15–17].

For the synthesis of $RE_4B_6O_{14}(OH)_2$ (RE = Dy, Ho) the assemblies were compressed in 3 h to 8.0 GPa and heated up to 880 °C in the following 10 min. After holding this temperature for 10 min, the samples were quenched to room temperature. After decompression the recovered experimental octahedrons were broken apart and the samples carefully separated from the surrounding BN. The products were obtained as coarsely crystalline solids (yield: 50 mg per run). $Dy_4B_6O_{14}(OH)_2$ is colorless, whereas the color of $Ho_4B_6O_{14}(OH)_2$ depends on the light source. In daylight, $Ho_4B_6O_{14}(OH)_2$ has a light beige color, while in the laboratory (neon lamps) it appears bright pink (Alexandrite-effect) [18].

In principle, the described hydrogen containing components $RE_4B_6O_{14}(OH)_2$ (RE = Dy, Ho) represent intermediates on the way to the hydrogen free rare-earth oxoborates $RE_4B_6O_{15}$ (RE = Dy, Ho) [5–7] by elimination of water (Eq. (2)):

$$RE_4B_6O_{14}(OH)_2\ (RE = Dy,\ Ho) \xrightarrow[>1000\,^\circ C]{8.0\ GPa} RE_4B_6O_{15}\ (RE = Dy,\ Ho) + H_2O. \tag{2}$$

In a series of 22 experiments, starting with the composition Dy_2O_3:B_2O_3 = 2:3 thoroughly mixed under air, we were able to find out the optimal conditions for the synthesis of the hydrogen containing oxoborate $Dy_4B_6O_{14}(OH)_2$. The systematic analysis of the X-ray powder patterns exhibited different stability ranges depending on pressure and temperature. The following trends were observed: for the synthesis of $Dy_4B_6O_{14}(OH)_2$ a minimum pressure of 7.7 GPa was necessary. Beneath this pressure, we observed the formation of β-$Dy_2B_4O_9$ [10] next to π-$DyBO_3$ [19]. Increasing the pressure up to 10 GPa had no significant effect on the synthesis in contrast to the variation of temperature. Temperatures larger than 1000 °C led directly to the hydrogen free component $Dy_4B_6O_{15}$. Lowering the temperature in the area of 900–950 °C led

to a phase mixture between $Dy_4B_6O_{15}$ and $Dy_4B_6O_{14}(OH)_2$. By further lowering into the temperature range of 850–900 °C, we obtained nearly exclusively $Dy_4B_6O_{14}(OH)_2$.

Next to the temperature range, there exists another dependence upon the heating time. Short times (2 min at 1000 °C) brought mixtures of $Dy_4B_6O_{15}$ and $Dy_4B_6O_{14}(OH)_2$, whereas long times (10 min at 1000 °C) led to $Dy_4B_6O_{15}$, confirming the progress of the decomposition-reaction (Eq. (2)). Knowing this, the direct synthesis of $Dy_4B_6O_{14}(OH)_2$ and the isotypic phase $Ho_4B_6O_{14}(OH)_2$ succeeded directly at 8 GPa and 880 °C (10 min) without any problems.

All these observations confirm that the new rare-earth oxoborates $RE_4B_6O_{14}(OH)_2$ (RE = Dy, Ho) represent tangible intermediate stages on the way to $RE_4B_6O_{15}$ (RE = Dy, Ho).

3. Crystal structure analysis

The powder diffraction data of $RE_4B_6O_{14}(OH)_2$ (RE = Dy, Ho) were collected on a STOE Stadi P powder diffractometer with monochromatized Cu$K\alpha_1$ radiation. The pattern of $Dy_4B_6O_{14}(OH)_2$ exhibited a second phase, which was identified as χ-$DyBO_3$ [3]. In the case of $Ho_4B_6O_{14}(OH)_2$, the powder pattern showed additional reflections, which could not be assigned until now. The corresponding reflections of the phases $RE_4B_6O_{14}(OH)_2$ (RE = Dy, Ho) were indexed with the program TREOR [20]. The lattice parameters ($Dy_4B_6O_{14}(OH)_2$: $a = 1293.9(2)$, $b = 437.54(4)$, $c = 888.25(9)$ pm; $Ho_4B_6O_{14}(OH)_2$: $a = 1292.6(2)$, $b = 436.22(3)$, $c = 887.11(7)$ pm (Table 1)) were obtained from least square fits of the powder data. The correct indexing of the pattern was ensured by intensity calculations [21], taking the atomic positions from the structure refinements. The lattice parameters determined by the powders and the single crystals agreed well (Table 1).

Small single crystals were isolated by mechanical fragmentation and examined by Buerger precession photographs from both phases. Single crystal intensity data were collected from regularly shaped crystals at 293 K by use of an Enraf–Nonius Kappa CCD, equipped with a rotating anode (Mo$K\alpha$ radiation ($\lambda = 71.073$ pm)). A numerical absorption correction (HABITUS [22]) was applied to the data. All relevant information concerning the data collections are listed in Table 1. In the case of $Dy_4B_6O_{14}(OH)_2$ the measurement took place with double redundancy, so the total number of measured reflections is about twice as high as in the case of $Ho_4B_6O_{14}(OH)_2$. According to the systematic extinctions $0kl$ with $k \neq 2n$, $h0l$ with $l \neq 2n$, and $hk0$ with $h + k \neq 2n$, the space group *Pbcn* (No. 60) was derived. The starting positional parameters were deduced from an automatic interpretation of direct methods with SHELXS-97 [23], and all non-hydrogen atoms were refined successfully with anisotropic atomic displacement parameters, using SHELXL-97 (full-matrix least-squares on F^2) [24]. Final difference Fourier syntheses did not reveal any significant residual peaks (see Table 1). The positional parameters and interatomic distances of the refinements are listed in Tables 2–6. Listings of the observed/calculated structure factors and other details are available from the Fachinformationszentrum Karlsruhe, D-76344 Eggenstein-Leopoldshafen (Germany), E-mail: crysdata@fiz-karlsruhe.de, by quoting the registry number CSD-413927 for $Dy_4B_6O_{14}(OH)_2$ and CSD-413928 for $Ho_4B_6O_{14}(OH)_2$.

4. Results and discussion

Due to the pressure coordination rule, the crystal structure of the new high-pressure rare-earth oxoborates $RE_4B_6O_{14}(OH)_2$ (RE = Dy, Ho) (Figs. 1 and 2) is built up exclusively from BO_4-tetrahedra. In contrast to the hydrogen-free compounds $RE_4B_6O_{15}$ (RE = Dy, Ho) [5–7], in which one third of the BO_4-tetrahedra are connected via common edges, the tetrahedra in $RE_4B_6O_{14}(OH)_2$ (RE = Dy, Ho) share common vertices only. In detail, the BO_4-tetrahedra form eight-membered rings (Fig. 1), which are condensed to layers within the *ab*-plane. Fig. 2 gives a view of these layers stacked along *c*. The eight-membered rings, characterized by the descriptor "$\langle 8\square \rangle$", represent a possible fundamental building block (FBB) for the description of the layered structure of $RE_4B_6O_{14}(OH)_2$ (RE = Dy, Ho) as proposed by Burns et al. [25,26]. A comparison with an enumeration of borate minerals based on infinite sheets of polyhedra, which can be found in reference [27], contains no example for this descriptor. Between the layers, the *RE*-atoms are positioned, coordinated by 7 + 2 oxygen atoms of the BO_4-tetrahedra, in a distance of 230–288 pm for both compounds. Fig. 3 shows the coordination sphere of the rare-earth cations. The distances of the nearest seven oxygen atoms range between 230 and 240 pm, whereas the two additional oxygen atoms (O2*b* and O2*c*; Table 3) possess a distance between 280 and 289 pm. MAPLE-calculations (Madelung Part of Lattice Energy) [28–30] confirmed the weak coordinative contribution of these two oxygen-atoms, therefore it is justified to speak of a 7 + 2 coordination sphere. The next oxygen atom in the coordination sphere of the rare-earth cations appears in a distance of 325 pm, having no considerable contribution. The distances *RE*–O correspond to values found before in high-pressure phases like χ-$DyBO_3$ (CN of Dy^{3+}: 7, 8, and 9; range: 219–272 pm) [3], β-$Dy_2B_4O_9$ (CN of Dy^{3+}: 9 and 10; range: 226–266 pm) [10], $RE_4B_6O_{15}$ (RE = Dy, Ho) (CN of RE^{3+}: 8; range:

Table 1
Crystal data and structure refinement for $RE_4B_6O_{14}(OH)_2$ (RE = Dy, Ho)

Empirical formula	$Dy_4B_6O_{14}(OH)_2$		$Ho_4B_6O_{14}(OH)_2$
Molar mass ($g\,mol^{-1}$)	972.88		982.60
Crystal system		Orthorhombic	
Space group		*Pbcn* (No. 60)	
Powder diffractometer		Stoe Stadi P	
Radiation		Cu$K\alpha_1$ ($\lambda = 154.06$ pm)	
Powder diffraction data			
a (pm)	1293.9(2)		1292.6(2)
b (pm)	437.54(4)		436.22(3)
c (pm)	888.25(9)		887.11(7)
Volume (nm^3)	0.503(1)		0.500(1)
Single crystal diffractometer		Enraf–Nonius Kappa CCD	
Radiation		Mo$K\alpha$ ($\lambda = 71.073$ pm)	
Single crystal data			
a (pm)	1292.7(2)		1292.8(2)
b (pm)	437.1(2)		436.2(2)
c (pm)	887.3(2)		887.1(2)
Volume $(nm)^3$	0.502(1)		0.500(1)
Formula units per cell		$Z = 2$	
Temperature (K)	293(2)		293(2)
Calculated density ($g\,cm^{-3}$)	6.442		6.523
Crystal size (mm^3)	$0.015 \times 0.03 \times 0.05$		$0.02 \times 0.02 \times 0.02$
Detector distance (mm)	30.0		30.0
Exposure time per (deg/s)	120		120
Absorption coefficient (mm^{-1})	29.57		31.41
$F(000)$	848		856
θ range (deg)	4.6–30.0		3.2–30.0
Range in $h\,k\,l$	$\pm 18, \pm 6, \pm 12$		$\pm 18, -5/+6, -12/+11$
Scan type	φ/ω		φ/ω
Total no. reflections	12727		6263
Independent reflections	727 ($R_{int} = 0.0455$)		728 ($R_{int} = 0.0372$)
Reflections with $I > 2\sigma(I)$	668 ($R_\sigma = 0.0217$)		673 ($R_\sigma = 0.0297$)
Parameters	61		61
Absorption correction		Numerical (HABITUS [22])	
Transm. ratio (max/min)	0.7936/0.4641		0.2659/0.1934
Goodness-of-fit (F^2)	1.141		1.161
Final R indices [$I > 2\sigma(I)$]	$R_1 = 0.0163$		$R_1 = 0.0177$
	w$R_2 = 0.0340$		w$R_2 = 0.0398$
R indices (all data)	$R_1 = 0.0190$		$R_1 = 0.0206$
	w$R_2 = 0.0349$		w$R_2 = 0.0406$
Extinction coefficient	0.0017(2)		0.0012(2)
Larg. diff. peak a. hole ($e\,Å^{-3}$)	1.80/−1.01		1.44/−1.06

222–265 pm) [6], and β-$RE_2B_4O_9$ (RE = Eu, Gd, Tb) (CN of RE^{3+}: 8–11; range: 223–307 pm) [9].

In the tetrahedral BO_4-groups of $RE_4B_6O_{14}(OH)_2$ (RE = Dy, Ho), the B–O distances shift between 143 and 151 pm (RE = Dy) and 143–152 pm (RE = Ho) with an average value of 149.1 pm (Table 4). This value is slightly higher than the average B–O distance of 147.6 pm in tetrahedral BO_4-units of oxoborates [27,31]. The O–B–O angles in the two crystallographically independent BO_4-tetrahedra vary between 103° and 112° in both compounds with an average value of 109.5°.

Due to the presence of the heavy rare-earth cations Dy^{3+} and Ho^{3+}, a localization of hydrogen atoms on the basis of the Fourier difference map was not possible. Nevertheless, geometrical reasons and bond-valence calculations indicate the possible positions of the hydrogen atoms. Fig. 4 gives a separate view of the environments of the four crystallographically distinguishable oxygen atoms (O1–O4) and their location inside the layer. The atom O1 has a distorted tetrahedral coordination sphere, built up from one boron and three dysprosium atoms. O2 is coordinated from one dysprosium and two boron atoms plus two dysprosium atoms in the second coordination sphere (O2-Dy1a: 236.5(3) pm; O2-Dy1b: 280.9(3) pm; O2-Dy1c: 288.3(3) pm) (values for $Ho_4B_6O_{14}(OH)_2$ see Table 4). The equally spaced coordination spheres of O1 and O2 (Fig. 4 top)

Table 2
Atomic coordinates and anisotropic displacement parameters/Å^2 for $Dy_4B_6O_{14}(OH)_2$ (space group *Pbcn*)

Atom	Wyckoff-position	x	y	z	U_{eq}	
Dy1	8*d*	0.14042(2)	0.04327(4)	0.53949(2)	0.0073(1)	
O1	8*d*	0.3108(2)	0.0362(6)	0.4646(4)	0.0061(5)	
O2	8*d*	0.2175(2)	0.2109(6)	0.2462(3)	0.0068(5)	
O3	8*d*	0.9061(2)	0.6369(6)	0.2592(3)	0.0074(5)	
O4	8*d*	0.9962(2)	0.2456(7)	0.1094(3)	0.0106(6)	
B1	4*c*	0	0.441(2)	1/4	0.010(2)	
B2	8*d*	0.3069(4)	0.0247(10)	0.3033(5)	0.0069(8)	
Atom	U_{11}	U_{22}	U_{33}	U_{23}	U_{13}	U_{12}
Dy1	0.0083(2)	0.0060(2)	0.0077(2)	0.00054(6)	0.00129(6)	0.00070(6)
O1	0.009(2)	0.003(2)	0.006(2)	0.000(1)	−0.001(1)	−0.002(1)
O2	0.007(2)	0.006(2)	0.008(2)	−0.001(1)	−0.002(1)	0.001(1)
O3	0.007(2)	0.005(2)	0.011(2)	−0.002(2)	0.001(2)	−0.000(1)
O4	0.009(2)	0.012(2)	0.012(2)	−0.005(2)	−0.001(2)	0.001(2)
B1	0.001(3)	0.009(3)	0.019(3)	0	0.000(2)	0
B2	0.007(2)	0.005(2)	0.009(2)	0.001(2)	0.000(2)	0.000(2)

U_{eq} is defined as one third of the trace of the orthogonalized U_{ij} tensor.

Table 3
Atomic coordinates and anisotropic displacement parameters/Å^2 for $Ho_4B_6O_{14}(OH)_2$ (space group *Pbcn*)

Atom	Wyckoff-position	x	y	z	U_{eq}	
Ho1	8*d*	0.14036(2)	0.04323(5)	0.5392(2)	0.0079(1)	
O1	8*d*	0.3109(3)	0.0358(7)	0.4647(3)	0.0067(6)	
O2	8*d*	0.2169(2)	0.2077(7)	0.2466(3)	0.0069(6)	
O3	8*d*	0.9060(2)	0.6381(7)	0.2598(3)	0.0077(6)	
O4	8*d*	0.9957(2)	0.2434(7)	0.1088(3)	0.0119(6)	
B1	4*c*	0	0.439(2)	1/4	0.006(2)	
B2	8*d*	0.3066(4)	0.0250(10)	0.3035(6)	0.0069(9)	
Atom	U_{11}	U_{22}	U_{33}	U_{23}	U_{13}	U_{12}
Ho1	0.0091(2)	0.0065(2)	0.0080(2)	0.00072(7)	0.00133(7)	0.00073(7)
O1	0.008(2)	0.006(2)	0.006(2)	−0.001(2)	−0.001(2)	−0.001(2)
O2	0.007(2)	0.005(2)	0.008(2)	−0.002(2)	−0.002(2)	0.001(2)
O3	0.005(2)	0.007(2)	0.011(2)	−0.002(2)	0.001(2)	0.000(2)
O4	0.010(2)	0.014(2)	0.012(2)	−0.004(2)	−0.002(2)	0.000(2)
B1	0.001(3)	0.007(3)	0.011(3)	0	−0.001(2)	0
B2	0.008(2)	0.003(2)	0.010(2)	−0.00(2)	0.001(2)	0.002(2)

U_{eq} is defined as one third of the trace of the orthogonalized U_{ij} tensor.

Table 4
Interatomic *RE*–O–distances (*RE* = Dy, Ho)/pm, calculated with the single crystal lattice parameters in $RE_4B_6O_{14}(OH)_2$ (*RE* = Dy, Ho) (standard deviations in parentheses)

Dy1–O1a	230.0(3)	Ho1–O1a	230.1(3)
Dy1–O4a	233.5(3)	Ho1–O4a	233.2(3)
Dy1–O1b	234.1(3)	Ho1–O1b	233.5(3)
Dy1–O3	234.7(3)	Ho1–O3	233.9(3)
Dy1–O2a	236.5(3)	Ho1–O2a	235.8(3)
Dy1–O4b	237.7(3)	Ho1–O4b	236.3(3)
Dy1–O1c	239.8(3)	Ho1–O1c	239.5(3)
Dy1–O2b	280.9(3)	Ho1–O2b	282.3(3)
Dy1–O2c	288.3(3)	Ho1–O2c	287.0(3)

make an additional bonded hydrogen atom highly improbable. The oxygen O3 represents a bridging atom O[2], giving also a coordinative contribution to Dy1 (distorted trigonal coordination). In contrast, O4 represents a terminal oxygen atom O[1] with a coordinative contribution to two dysprosium atoms (Fig. 4 bottom right). The coordinative situation favors the assumption, that the hydrogen atoms are bound to O4. This is supported by a comparison of the boron–oxygen bond distances, where the distance B1–O4 appears as the longest one (151.2(5) pm in $Dy_4B_6O_{14}(OH)_2$ and 151.7(5) pm in $Ho_4B_6O_{14}(OH)_2$). Bond-valence sums, using the bond-length/bond-strength concept (Dy_4

Table 5
Interatomic B–O–distances (RE = Dy, Ho)/pm, calculated with the single crystal lattice parameters in $RE_4B_6O_{14}(OH)_2$ (RE = Dy, Ho) (standard deviations in parentheses)

$Dy_4B_6O_{14}(OH)_2$				$Ho_4B_6O_{14}(OH)_2$			
B1–O3	148.8(5) 2 ×	B2–O1	143.4(5)	B1–O3	149.6(5) 2 ×	B2–O1	143.2(6)
B1–O4	151.2(5) 2 ×	B2–O3	148.1(5)	B1–O4	151.7(5) 2 ×	B2–O3	148.6(7)
		B2–O2a	149.6(5)			B2–O2a	149.5(6)
		B2–O2b	150.2(5)			B2–O2b	150.5(5)
	∅ = 150.0		∅ = 147.8		∅ = 150.7		∅ = 148.0

Table 6
Interatomic angles (deg) calculated with the single crystal lattice parameters in $RE_4B_6O_{14}(OH)_2$ (RE = Dy, Ho) (standard deviations in parentheses)

$Dy_4B_6O_{14}(OH)_2$			
O3–B1–O3	109.6(5)	O1–B2–O3	109.4(3)
O3–B1–O4	110.1(2) 2 ×	O1–B2–O2	112.2(3)
O3–B1–O4	107.8(2) 2 ×	O3–B2–O2	111.1(3)
O4–B1–O4	111.4(5)	O1–B2–O2	110.2(3)
		O3–B2–O2	111.1(3)
		O2–B2–O2	102.7(3)
	∅ = 109.5		∅ = 109.5
$Ho_4B_6O_{14}(OH)_2$			
O3–B1–O3	109.2(5)	O1–B2–O3	109.5(4)
O3–B1–O4	107.9(2) 2 ×	O1–B2–O2	110.5(4)
O3–B1–O4	110.2(2) 2 ×	O3–B2–O2	111.5(3)
O4–B1–O4	111.4(5)	O1–B2–O2	111.9(3)
		O3–B2–O2	110.7(3)
		O2–B2–O2	102.7(3)
	∅ = 109.5		∅ = 109.5

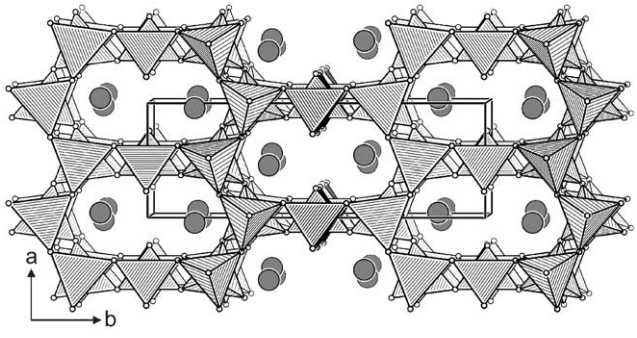

Fig. 1. Crystal structure of $RE_4B_6O_{14}(OH)_2$ (RE = Dy, Ho). View along [001]. The rare-earth cations are shown as large gray spheres and oxygens as white spheres.

$B_6O_{14}(OH)_2$: O1: −2.03; O2: −1.99; O3: −1.85; O4: −1.45) and the CHARDI concept ($Dy_4B_6O_{14}(OH)_2$: O1: −2.15; O2: −1.88; O3: −1.95; O4: −1.53), confirm the special position of O4 with a significant deviation from the value −2 in contrast to all other atoms, which are in agreement within the limits of the concepts [32–34].

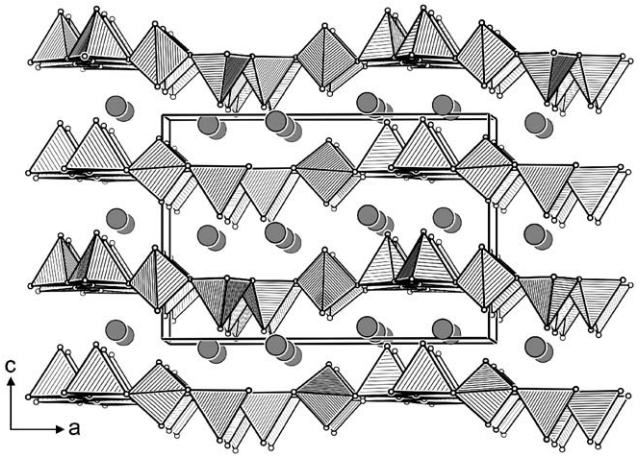

Fig. 2. Crystal structure of $RE_4B_6O_{14}(OH)_2$ (RE = Dy, Ho). View along [010]. The rare-earth cations are shown as large grey spheres and oxygens as white spheres.

4.1. In situ powder diffraction and thermoanalytical measurements

To investigate the metastable character of the high-pressure phases $RE_4B_6O_{14}(OH)_2$ (RE = Dy, Ho), temperature-dependent measurements were performed on a STOE powder diffractometer Stadi P (Mo $K\alpha$; $\lambda = 71.073$ pm) with a computer-controlled STOE furnace. The heating element consisted of an electrically heated graphite tube, holding the sample capillary vertically related to the scattering plane. Bores in the graphite tube permitted unobstructed pathways for the primary beam as well as for the scattered radiation. The temperature, measured by a thermocouple in the graphite tube, was kept constant within 0.2 °C. The heating rate between different temperatures was set to 22 °C/min. For temperature stabilization, a time of three minutes was given before the start of each data acquisition.

Successive heating of the metastable high-pressure phase $Dy_4B_6O_{14}(OH)_2$ (Fig. 5) led to a slow decomposition at temperatures larger than 300 °C, followed by an entire decomposition in the range of 700–800 °C into the high-temperature orthoborate μ-$DyBO_3$ [19] and

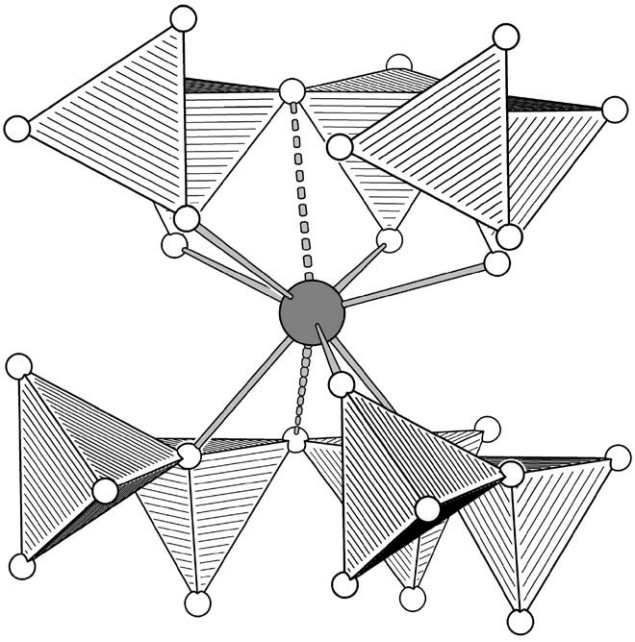

Fig. 3. Coordination of RE^{3+} in the crystal structure of $RE_4B_6O_{14}(OH)_2$ (RE = Dy, Ho).

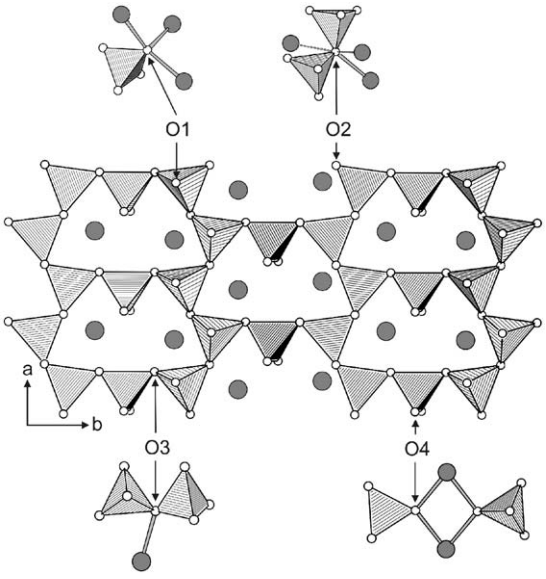

Fig. 4. Single layer of condensed BO_4-tetrahedra in $RE_4B_6O_{14}(OH)_2$ (RE = Dy, Ho) with plots of the coordination spheres of the four crystallographically independent oxygen atoms.

presumable liquid B_2O_3 according to Eq. (3):

$$RE_4B_6O_{14}(OH)_2\ (RE = \mathrm{Dy},\ \mathrm{Ho}) \xrightarrow{\Delta T} 4RE BO_3$$

$$(RE = \mathrm{Dy},\ \mathrm{Ho}) + B_2O_3 + H_2O. \quad (3)$$

In the decomposition area at 700 °C, one can guess the weak appearance of the normal temperature phase

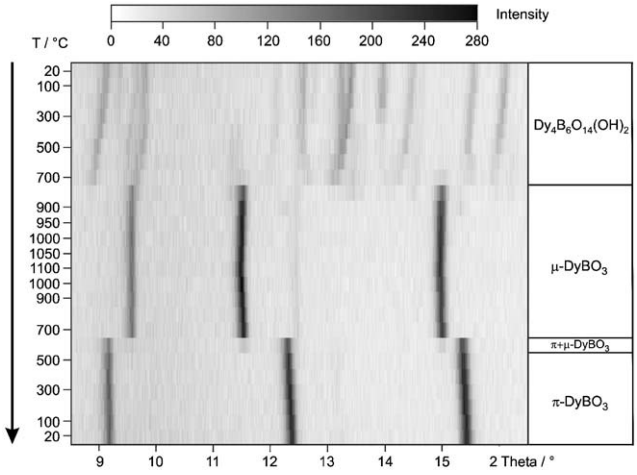

Fig. 5. Temperature dependent X-ray thermodiffractometric powder patterns of the decomposition of $Dy_4B_6O_{14}(OH)_2$.

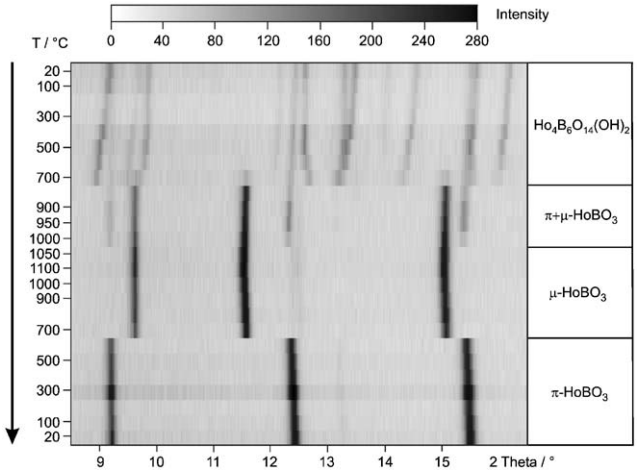

Fig. 6. Temperature dependent X-ray thermodiffractometric powder patterns of the decomposition of $Ho_4B_6O_{14}(OH)_2$.

π-$DyBO_3$ [19,35]. This phase appeared again by further cooling below 700 °C.

In the case of the metastable high-pressure phase $Ho_4B_6O_{14}(OH)_2$ (Fig. 6), the decomposition starts around 400 °C, followed by the complete decomposition at 700–800 °C leading to $\pi + \mu$-$HoBO_3$ [19,35]. Above 1000 °C, only the high-temperature orthoborate μ-$HoBO_3$ was detectable. Cooling beneath 700 °C resulted in a transformation back to the room-temperature modification π-$HoBO_3$.

These results were approved by thermoanalytical measurements, which were performed with a combined DTA-TG-thermobalance (TGA 92-2400, Setaram, heating rate: 10 °C min^{-1}) between room temperature and 1000 °C for $Dy_4B_6O_{14}(OH)_2$ (Fig. 7). During heating, some weak exothermic effects were examined between 500 and 600 °C, followed by a characteristic

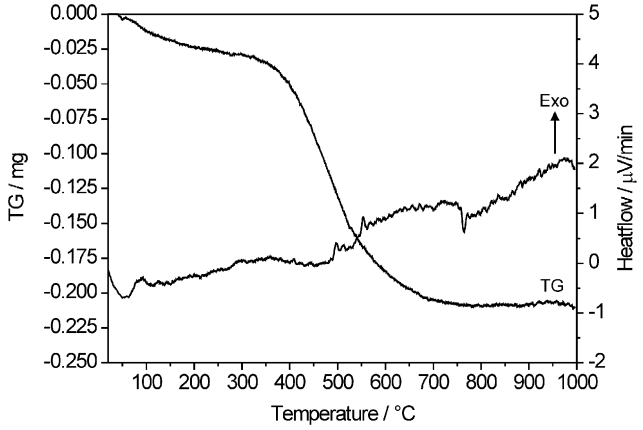

Fig. 7. Differential thermal analysis curve and thermogravimetrical curve of $Dy_4B_6O_{14}(OH)_2$.

endothermic effect in the DTA between 750 and 770 °C, due to the decomposition of the compound. At the same time, we were able to observe a weight loss of 1.36% between 110 and 800 °C, which corresponds to the quantitative loss of water from the starting composition $Dy_4B_6O_{14}(OH)_2$ (theoretical value: 1.85%). The difference between the observed and the calculated values comes from an impurity (χ-$DyBO_3$ [3]) in this specific sample, which was estimated to have a contribution of 25% on the basis of the powder data. This leads to a theoretical value of 1.39%, which is in agreement with the observed weight loss.

4.2. Infrared absorption spectroscopy

The infrared (IR) spectra of $RE_4B_6O_{14}(OH)_2$ (RE = Dy, Ho) were recorded on a Bruker IFS 66v/S spectrometer, scanning a range from 400 to 4000 cm^{-1}. The sample was thoroughly mixed with dried KBr (5 mg sample, 500 mg KBr) in a glove box under a dried argon atmosphere. Fig. 8 (top) shows the infrared spectrum of $Dy_4B_6O_{14}(OH)_2$, Fig. 8 (bottom) the spectrum of $Ho_4B_6O_{14}(OH)_2$. The absorption peaks between 1100 and 800 cm^{-1} are those typical for the tetrahedral borate groups BO_4, as in YBO_3, $GdBO_3$, or $TaBO_4$ [36–38]. In both spectra, it can be assumed that the absorptions between 1100 and 1000 cm^{-1} correspond to antisymmetric stretching modes ν_{as} (1017 cm^{-1} in $Dy_4B_6O_{14}(OH)_2$; 1013 cm^{-1} in $Ho_4B_6O_{14}(OH)_2$). Accordingly, the symmetric stretching modes ν_s can be found at 850 cm^{-1}. Both, the asymmetric and the symmetric absorptions exhibit shoulders, which can be attributed to two crystallographically distinguishable BO_4-tetrahedra. The presence of hydrogen in these phases is verified by the observation of deformation modes δ_{OH} at 1328 cm^{-1} ($Dy_4B_6O_{14}(OH)_2$) and 1335 cm^{-1} ($Ho_4B_6O_{14}(OH)_2$), accompanied by ν_{OH} (3500–3000 cm^{-1}), which are typical for hydroxyl groups in borates [39].

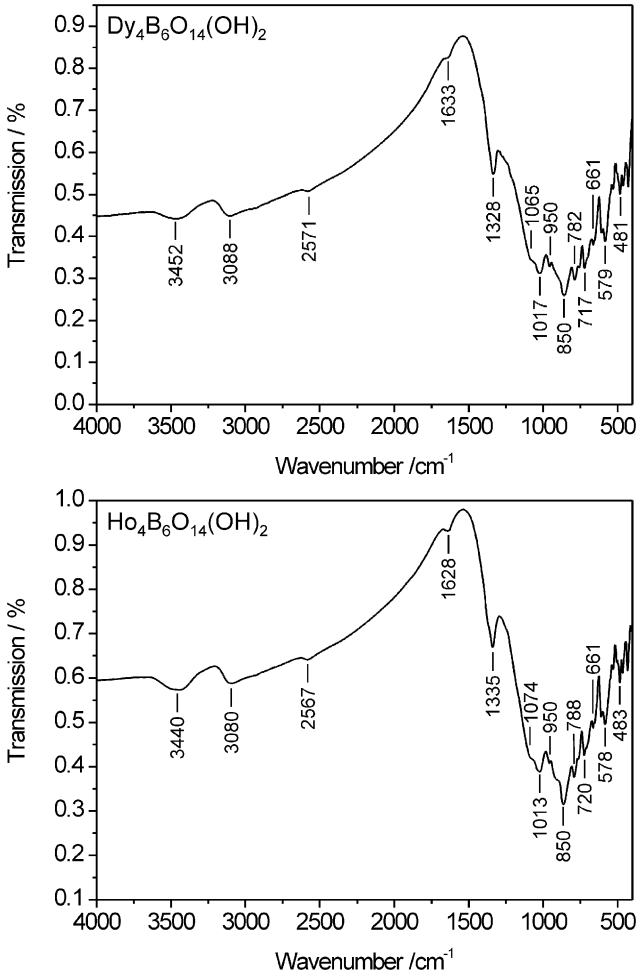

Fig. 8. Infrared spectra of $Dy_4B_6O_{14}(OH)_2$ (top) and $Ho_4B_6O_{14}(OH)_2$ (bottom).

5. Conclusion

In this paper, we described the multianvil-synthesis of the new rare-earth oxoborates $RE_4B_6O_{14}(OH)_2$ (RE = Dy, Ho) under extreme high-pressure/high-temperature conditions. The structures were solved from single crystal data. According to the pressure coordination rule, all boron atoms in the network exhibit exclusively tetrahedral oxygen coordination. Both phases represent intermediate compounds on the way to the formation of $RE_4B_6O_{15}$ (RE = Dy, Ho) [5–7]. For a detailed investigation of the stability ranges in dependence of pressure and temperature, we are going to perform in situ high-pressure/high-temperature experiments in the near future.

Acknowledgments

The author thanks Prof. Dr. W. Schnick, Department Chemie of the University of Munich (LMU), for his steady interest and continuous support of this work.

Special thanks go to Dr. H. Piotrowski for collecting the single crystal data, to Dipl. Chem. S. Correll for the in situ powder diffraction measurements, to Dipl. Chem. S. Schmid for the DTA/TG-measurements, and to Prof. Dr. B. Engelen (University of Siegen) for the fruitful discussions. This work was financially supported by the Deutsche Forschungsgemeinschaft.

References

[1] H. Huppertz, Z. Naturforsch. 56b (2001) 697.
[2] H. Huppertz, Z. Kristallogr. 219 (2004) 330.
[3] H. Huppertz, B. von der Eltz, R.-D. Hoffmann, H. Piotrowski, J. Solid State Chem. 166 (2002) 203.
[4] H. Emme, T. Nikelski, Th. Schleid, R. Pöttgen, M.H. Möller, H. Huppertz, Z. Naturforsch. 59b (2004) 202.
[5] H. Huppertz, B. von der Eltz, J. Am. Chem. Soc. 124 (2002) 9376.
[6] H. Huppertz, Z. Naturforsch. 58b (2003) 278.
[7] H. Huppertz, H. Emme, J. Phys.: Condens. Matter 16 (2004) S1283.
[8] H. Emme, H. Huppertz, Z. Anorg. Allg. Chem. 628 (2002) 2165.
[9] H. Emme, H. Huppertz, Chem. Eur. J. 9 (2003) 3623.
[10] H. Huppertz, S. Altmannshofer, G. Heymann, J. Solid State Chem. 170 (2003) 320.
[11] G.I. Vasil'ev, V.V. Serebrennikov, Russ. J. Inorg. Chem. 9 (1964) 1343.
[12] Sw. Pajakoff, Monatsh. Chem. 100 (1969) 1350.
[13] L. Li, P. Lu, Y. Wang, X. Jin, G. Li, Y. Wang, L. You, J. Lin, Chem. Mater. 14 (2002) 4963.
[14] L. Li, X. Jin, G. Li, Y. Wang, F. Liao, G. Yao, J. Lin, Chem. Mater. 15 (2003) 2253.
[15] D. Walker, M.A. Carpenter, C.M. Hitch, Am. Mineral. 75 (1990) 1020.
[16] D. Walker, Am. Mineral. 76 (1991) 1092.
[17] D.C. Rubie, Phase Trans. 68 (1999) 431.
[18] H.M. Farok, G.A. Saunders, W.A. Lambsom, R. Krüger, H.B. Senin, S. Bartlett, S. Takel, Phys. Chem. Glasses 37 (1996) 125.
[19] E.M. Levin, R.S. Roth, J.B. Martin, Am. Mineral. 46 (1961) 1030.
[20] P.-E. Werner, L. Eriksson, M. Westdahl, J. Appl. Crystallogr. 18 (1985) 367.
[21] WinX^{POW} Software, STOE & CIE GmbH, Darmstadt, 1998.
[22] W. Herrendorf, H. Bärnighausen, HABITUS, Program for Numerical Absorption Correction, University of Karlsruhe/Gießen, Germany, 1993/1997.
[23] G.M. Sheldrick, SHELXS-97, Program for the Solution of Crystal Structures, University of Göttingen, Germany, 1997.
[24] G.M. Sheldrick, SHELXL-97, Program for Crystal Structure Refinement, University of Göttingen, Germany, 1997.
[25] P.C. Burns, J.D. Grice, F.C. Hawthorne, Can. Mineral. 33 (1995) 1131.
[26] J.D. Grice, P.C. Burns, F.C. Hawthorne, Can. Mineral. 37 (1999) 731.
[27] F.C. Hawthorne, P.C. Burns, J.D. Grice, in: E.S. Grew, L.M. Anovitz (Eds.), Boron: Mineralogy, Petrology, and Geochemistry. Reviews in Mineralogy, Vol. 33, Mineralogical Society of America, Washington, 1996 (Chapter 2).
[28] R. Hoppe, Angew. Chem. 78 (1966) 52;
R. Hoppe, Angew. Chem. Int. Ed. Engl. 5 (1966) 95.
[29] R. Hoppe, Angew. Chem. 82 (1970) 7;
R. Hoppe, Angew. Chem. Int. Ed. Engl. 9 (1970) 25.
[30] R. Hübenthal, MAPLE, Program for the Calculation of MAPLE Values, Vers. 4, University of Giessen, Germany, 1993.
[31] E. Zobetz, Z. Kristallogr. 191 (1990) 45.
[32] I.D. Brown, D. Altermatt, Acta Crystallogr. B 24 (1985) 869.
[33] N.E. Breese, M. O'Keeffe, Acta Crystallogr. B 47 (1991) 192.
[34] R. Hoppe, S. Voigt, H. Glaum, J. Kissel, H.P. Müller, K. Bernet, J. Less-Common Met. 156 (1989) 105.
[35] R.E. Newnham, M.J. Redman, R.P. Santoro, J. Am. Chem. Soc. 46 (1963) 253.
[36] M. Ren, J.H. Lin, Y. Dong, L.Q. Yang, M.Z. Su, L.P. You, Chem. Mater. 11 (1999) 1576.
[37] J.P. Laperches, P. Tarte, Spectrochim. Acta 22 (1966) 1201.
[38] G. Blasse, G.P.M. van den Heuvel, Phys. Stat. Sol. 19 (1973) 111.
[39] K. Frey, E. Funck, Z. Naturforsch. 27b (1972) 101.